Using Chaos Theory to Analyze Particle Dynamics in Asymmetry-induced Transport

D.L. Eggleston[1,a)]

[1]*Occidental College, Physics Department, M-21, 1600 Campus Road, Los Angeles, CA, 90041, USA*

[a)]Corresponding author: dleggles@oxy.edu
URL: https://sites.oxy.edu/dleggles/eggleston/research.htm

Abstract. Despite a large body of experimental work on asymmetry-induced transport in non-neutral plasmas, the correct theory remains elusive. Previous work using single particle computer simulations has shown that the particle dynamics in such systems can be quite complex. In this paper, the techniques of chaos theory are employed in an effort to better understand these dynamics. The dynamical equations are re-conceptualized as describing time-independent trajectories in a four-dimensional space consisting of the radius r, rotating frame angle ψ, axial position z, and axial velocity v. Initial work includes identification of an integral of the motion, fixed-point analysis of the dynamical equations, the construction and interpretation of Poincaré sections to visualize the dynamics, and, for the case of chaotic motion, numerical calculation of the largest Lyapunov exponent using the technique of Benettin et. al.

Introduction

Our previous computer studies[1] of the asymmetry-induced dynamics of particles in our Malmberg-Penning trap with a biased center wire[2] have revealed motions that cannot be described by a simple perturbation theory. In addition to lab-frame trapped particle populations, there were indications of chaotic motion. In this paper we apply some of the methodologies of chaos theory to single-particle dynamics in our trap in an effort to better characterize these dynamics.

The geometry of our trap is cylindrical, so the usual cylindrical coordinates (r, θ, z) are natural, with the z origin at one end of the confinement region of length L and radius R. With the confining magnetic field in the $\hat{z}$-direction, the governing equations of motion are then

$$\begin{aligned} \dot{r} &= \frac{1}{B} E_\theta(r, \theta, z, t) \\ \dot{\theta} &= -\frac{1}{rB} E_r(r, \theta, z, t) \\ \ddot{z} &= \frac{q}{m} E_z(r, \theta, z, t). \end{aligned} \tag{1}$$

Here we have used the drift approximation for $\dot{r}$ and $\dot{\theta}$ whereas $\ddot{z}$ is simply given by Newton's second law. The components of the electric field are derivatives of the potential which we take to be made up of a radially dependent part $\phi_0(r)$ produced by the center wire bias and an asymmetry potential $\phi_1(r, \theta, z, t)$.

Chaos theory takes a geometric approach to dynamics by studying trajectories in an abstract n-dimensional space[3]. To this end, the equations of motion are cast as n first-order autonomous differential equations for n dynamical variables. The n dynamical variables define a point in an n-dimensional space referred to as state space or, in the context of Hamiltonian dynamics, phase space. In addition, the n differential equations define a unique direction for the trajectory at that point. The fact that the differential equations are autonomous (i.e., without explicit time dependence) means that the trajectories are time-independent.

To cast our equations in this form, we introduce the axial velocity $v = \dot{z}$ and note that in our experiment the variables θ and t come in the combination $\omega t - l\theta \equiv -l\psi$. Since the components of the electric field are derivatives of

Non-Neutral Plasma Physics X
AIP Conf. Proc. 1928, 020001-1–020001-6; https://doi.org/10.1063/1.5021566
Published by AIP Publishing. 978-0-7354-1620-8/$30.00

the potential ϕ, we obtain

$$\begin{aligned} \dot{r} &= -\frac{1}{rB}\frac{\partial\phi}{\partial\psi}(r,\psi,z) \\ \dot{\psi} &= -\frac{\omega}{l} + \frac{1}{rB}\frac{\partial\phi}{\partial r}(r,\psi,z) \\ \dot{v} &= -\frac{q}{m}\frac{\partial\phi}{\partial z}(r,\psi,z) \\ \dot{z} &= v. \end{aligned} \tag{2}$$

Thus our dynamics can be viewed as trajectories in the four-dimensional space formed by r, ψ, z, and v. Note, however, that the quantity

$$E = \frac{1}{2}mv^2 + q\phi(r,\psi,z) - \frac{q\omega B}{2l}r^2 \tag{3}$$

is a constant of the motion, as can be verified by calculating $\dot{E}$ and using Equs. (2). This means that the trajectories are constrained to remain on constant E 3-D hypersurfaces in the 4-D state space.

Analytical Results

To proceed, we must now specify the form of the potential $\phi(r,\psi,z)$. We use a form that is relevant to our experimental work:

$$\phi(r,\psi,z) = \phi_0(r) + \phi_1(r)\cos kz\cos(-l\psi). \tag{4}$$

Here $\phi_0(r)$ is produced by a biased wire along the axis of the trap, while the second term is a perturbing asymmetric potential produced by biased wall patches, with k and l being the axial and azimuthal wavenumbers, respectively. Using this in Equs. (2) and specifying $q = -e$ gives

$$\begin{aligned} \dot{r} &= -\frac{l}{rB}\phi_1(r)\cos kz\sin(-l\psi) \\ \dot{\psi} &= -\frac{\omega}{l} + \omega_R(r) + \frac{1}{rB}\frac{d\phi_1}{dr}\cos kz\cos(-l\psi) \\ \dot{v} &= -\frac{ek}{m}\phi_1(r)\sin kz\cos(-l\psi) \\ \dot{z} &= v \end{aligned} \tag{5}$$

where we have defined $\omega_R(r) \equiv \frac{1}{rB}\frac{d\phi_0}{dr}$, the azimuthal rotation frequency produced by the biased center wire.

We first note that Equs. (5) satisfy the *necessary conditions* for chaos[3]. These are 1) the presence of nonlinearity that couples at least some of the equations (provided by the sine and cosine terms) and 2) the number of equations minus the number of constants of motion must be greater than or equal to three (we have four equations and one constant given by Eq. (3)). Interestingly, chaos theory does not yet have a way to determine *sufficient conditions*. As we shall see, trajectories for our system can be either regular or chaotic depending on initial conditions.

We next consider the fixed (or equilibrium) points of Equs. (5), i.e., those points where $\dot{r}$, $\dot{\psi}$, $\dot{z}$, $\dot{v}$ are all zero. While these points constitute a very small portion of state space, their properties often give insights into the larger picture[4].

From the $\dot{z}$ equation, we see immediately that fixed points require $v = 0$. Similarly, from the $\dot{r}$ and $\dot{v}$ equations, $\cos kz\sin(-l\psi) = 0$ and $\sin kz\cos(-l\psi) = 0$ are required. These can be simultaneously satisfied in two ways: 1) $kz = 0, \pm\pi$ and $-l\psi = 0, \pm\pi$ (making $\sin kz$ and $\sin(-l\psi)$ zero) or 2) $kz = \pm\frac{\pi}{2}$ and $-l\psi = \pm\frac{\pi}{2}$ (making $\cos kz$ and $\cos(-l\psi)$ zero). Here we have restricted the domain of the sine and cosine functions to $-\pi$ to $+\pi$. Finally, we require $\dot{\psi} = 0$ which means that $\omega_R(r) - \frac{\omega}{l} + \frac{1}{rB}\frac{d\phi_1}{dr}\cos kz\cos(-l\psi) = 0$. For the case 1 fixed points this reduces to $\omega_R(r) - \frac{\omega}{l} \pm \frac{1}{rB}\frac{d\phi_1}{dr} = 0$ while the case 2 cases simply require $\omega_R(r) - \frac{\omega}{l} = 0$. Since ϕ_1 is typically small compared to ϕ_0, both of these cases set the requirement that $\omega \approx l\omega_R(r)$, which sets the value of r for the fixed points.

We next examine the stability of the fixed points by considering small displacements δr, $\delta\psi$, δv, and δz from these equilibria. Each of the equalities in Eq. (5) can be Taylor expanded in powers of these displacements. To first order in

the displacements, the result can be cast in matrix form:

$$\frac{d}{dt}\begin{pmatrix}\delta r\\ \delta\psi\\ \delta v\\ \delta z\end{pmatrix}=\begin{pmatrix}-C_r\cos kz\sin(-l\psi) & lC\cos kz\cos(-l\psi) & 0 & kC\sin kz\sin(-l\psi)\\ \omega_r+D_r\cos kz\cos(-l\psi) & lD\cos kz\sin(-l\psi) & 0 & -kD\sin kz\cos(-l\psi)\\ -F_r\sin kz\cos(-l\psi) & -lF\sin kz\sin(-l\psi) & 0 & -kF\cos kz\cos(-l\psi)\\ 0 & 0 & 1 & 0\end{pmatrix}\begin{pmatrix}\delta r\\ \delta\psi\\ \delta v\\ \delta z\end{pmatrix} \tag{6}$$

where $C=\frac{1}{rB}\phi_1(r)$, $D=\frac{1}{rB}\frac{d\phi_1}{dr}$, $F=\frac{ek}{m}\phi_1(r)$, $C_r=\frac{dC}{dr}$, $D_r=\frac{dD}{dr}$, $F_r=\frac{dF}{dr}$, and $\omega_r=\frac{d\omega_R}{dr}$, and where the elements of the 4×4 matrix are evaluated at the fixed point under consideration. If we denote the column vector (δr,$\delta\psi$,δv,δz) as $\delta\mathbf{r}$ and the matrix as $\mathbf{J}$, we can write Eq. (6) in the compact form

$$\delta\dot{\mathbf{r}}=\mathbf{J}\delta\mathbf{r}. \tag{7}$$

$\mathbf{J}$ is called the Jacobian or stability matrix. Equation (7) can be solved by solving an associated eigenvalue problem[4]. To see this, assume that $\delta\mathbf{r}$ has the form

$$\delta\mathbf{r}=\sum_{i=1}^{4}c_i\mathbf{A_i}e^{\lambda_i t} \tag{8}$$

where c_i and λ_i are constants and $\mathbf{A_i}$ are constant four-vectors. Then

$$\mathbf{J}\delta\mathbf{r}=\mathbf{J}\sum_{i=1}^{4}c_i\mathbf{A_i}e^{\lambda_i t}=\sum_{i=1}^{4}c_i\mathbf{J}\mathbf{A_i}e^{\lambda_i t}. \tag{9}$$

The last expression is equal to $\delta\dot{\mathbf{r}}$ if $\mathbf{J}\mathbf{A_i}=\lambda_i\mathbf{A_i}$, that is, if $\mathbf{A_i}$ and λ_i are eigenvector and eigenvalue for the transformation $\mathbf{J}$. The solution of Eq. (7) can thus be found by finding these eigenvectors and eigenvalues and plugging into Eq. (8). The eigenvalues are found by solving the characteristic equation of the matrix $\mathbf{J}$, i.e., the determinant $|\mathbf{J}-\lambda\mathbf{I}|=\mathbf{0}$, which, in our case, gives four values λ_i. When each of these values is substituted into the eigenvalue equation, we obtain the corresponding eigenvector $\mathbf{A_i}$.

When the stability matrix is evaluated at the fixed points, the sine and cosine terms will give zero or ±1. For the case 1 fixed points, $\mathbf{J}$ reduces to

$$\begin{pmatrix}0 & lCS & 0 & 0\\ -G & 0 & 0 & 0\\ 0 & 0 & 0 & -kFS\\ 0 & 0 & 1 & 0\end{pmatrix} \tag{10}$$

where $-G=\omega_r+D_rS$ and the sign parameter $S=1$ when $(kz,-l\psi)$ are either $(0,0)$ or $(\pm\pi,\pm\pi)$, while $S=-1$ when $(kz,-l\psi)$ are either $(0,\pm\pi)$ or $(\pm\pi,0)$. The resulting eigenvalues are $[-i\sqrt{kFS},i\sqrt{kFS},-i\sqrt{lCGS},i\sqrt{lCGS}]$ with corresponding eigenvectors $[(0,0,-i\sqrt{kFS},1),(0,0,i\sqrt{kFS},1),(i\sqrt{lCS/G},1,0,0),(-i\sqrt{lCS/G},1,0,0)]$. We first note that, because of the zeros in the eigenvectors, the motion in the $r-\psi$ plane is independent of the motion in the $v-z$ plane. Secondly, since we have defined C, F, and G to be positive for typical experimental conditions, the character of the case 1 solutions thus depends only on the sign parameter S. For $S=1$ (case 1a), the eigenvalues are all imaginary. Such a fixed point is termed elliptical (or a center) since the resulting solutions can be cast in the form of ellipses in the $r-\psi$ and $v-z$ planes, with the rate of rotation about the center determined by the appropriate eigenvalue. For $S=-1$ (case 1b), the eigenvalues are all real, giving so-called hyperbolic (or saddle) points. Here the solutions can be cast in the form of hyperbolas in the $r-\psi$ and $v-z$ planes. Analysis of the $r-\psi$ motion shows that the flow is toward the origin in the first and third quadrants of the $r-\psi$ plane and away from the origin in the second and fourth quadrants. For the $v-z$ motion, the flow directions are reversed.

For the case 2 fixed points, $\mathbf{J}$ reduces to

$$\begin{pmatrix}0 & 0 & 0 & kCS\\ -H & 0 & 0 & 0\\ 0 & -lFS & 0 & 0\\ 0 & 0 & 1 & 0\end{pmatrix} \tag{11}$$

where $-H=\omega_r$ and $S=1$ when $(kz,-l\psi)$ are either $(\pi/2,\pi/2)$ or $(-\pi/2,-\pi/2)$, while $S=-1$ when $(kz,-l\psi)$ are either $(\pi/2,-\pi/2)$ or $(-\pi/2,\pi/2)$. The resulting eigenvalues are [$-R$,$-iR$,iR,R] with corresponding eigenvectors $[(-Q,-T,-R,1),(iQ,T,-iR,1),(-iQ,T,iR,1),(Q,-T,R,1)]$. Here we have defined $R=(HkClF)^{1/4}$, $Q=$

$(k^3C^3/HlF)^{1/4}$, and $T = (HkC/lF)^{1/2}$ for compactness, all of which are real for typical experimental conditions. Note that here the sign parameter S has cancelled out, so all case 2 solutions have the same character. Here the motion is more difficult to characterize, but the form of the eigenvalues and eigenvectors shows that the motion is fully four-dimensional with a mixture of elliptical and hyperbolic elements.

Numerical Results

We now turn to results obtained by numerically solving Equs. (5). To do so, we must specify further details of our model. The potential $\phi_0(r)$ is given by $\phi_{cw} \ln(R/r)/\ln(R/a)$, where ϕ_{cw} and a are the bias and radius of the center wire, respectively. The asymmetry potential $\phi_1(r)$ is given by $\phi_{10}(r/R)^l$, with ϕ_{10} a constant. The axial wavenumber $k = n\pi/L$, with n being an integer. For the results shown in this paper we use typical experimental values: $B = 364$ G, $\phi_{cw} = -80$ V, $l = k = 1$, $\omega = 0.5$, $\phi_{10} = 0.2$ V, and $\ln(R/a) = 5.3838$.

Numerical solutions are obtained using Mathematica's NDSOLVE routine. We treat our system as having infinite extent in z with periodicity $2L$, which is equivalent to assuming specular reflection at the ends of our confinement region of length L. We use the following scalings for our solutions: r is scaled to the wall radius R, z to L, v to $v_0 = 10^6$ cm/s, time t to 10^{-6} s, and frequencies to either 10^6 Hz (for λ) or 10^6 rad/s (for ω).

To check the accuracy of our solutions, we plug the resulting numerical functions for r, ψ, z and v back into Equs. (5) and take the difference between the two sides. A perfect solution would give zero for each equation. Judicious choices among NDSOLVE's options keep these quantities below 10^{-10} for our solutions, while variations in the constant E are in the range $\delta E/E \approx 10^{-6}$.

While the fixed point analysis in the previous section gives some indication of the types of motion to expect, we want to be able to characterize the motion for an arbitrary initial point in state space. Chaotic dynamics are characterized by the exponential divergence of neighboring initial points. The rate of divergence is given by the Lyapunov exponents, one for each dimension of the state space. The standard conceptual picture is to imagine a point in state space surrounded by a small sphere whose surface represents neighboring initial conditions. As the system evolves, the central point will follow its trajectory while the surface of the sphere will deform into an ellipsoid as the sphere stretches or contracts along its axes. The average rates of change along the axes are the Lyapunov exponents λ_i, defined by

$$\lambda_i = \lim_{t\to\infty, d_i(0)\to 0} \left[\frac{1}{t} \ln\left(\frac{d_i(t)}{d_i(0)} \right) \right] \tag{12}$$

where $d_i(t)$ is the length of the ellipsoid along the i^{th} axis at time t. The presence of chaos is then indicated by a positive λ_i. While this formal definition is widely quoted, it is not of much use in numerical calculations. Since the motion is bounded, $d_i(t)$ will quickly reach its maximum value, after which the $1/t$ factor will decrease λ_i to zero. An alternate method for calculating the largest Lyapunov exponent was developed by Benettin et. al[5]. The idea is to follow two neighboring trajectories separated by an initial small distance d_0 for a time τ, after which the distance between them is renormalized to its initial small value. The computation is then continued until a time 2τ, at which point the renormalization is repeated, and so on at time intervals of τ. At each multiple k of τ, the partial sum

$$\lambda_k = \frac{1}{k\tau} \sum_{j=1}^{k} \ln\left(\frac{d_j}{d_0} \right) \tag{13}$$

is computed, where d_j is the distance between the two trajectories before normalization. Then the maximum Lyapunov exponent is given by

$$\lambda = \lim_{k\to\infty} \lambda_k \tag{14}$$

which can be estimated by plotting λ_k versus k. Example plots are shown in Fig. 1. For both the cases shown, we have taken the initial conditions to be $v = 10$, $\psi = 0$, and $z = -0.05$. The solid circles have initial $r/R = 0.674$ while the open circles have 0.750. The numerical solutions extend only to $k = 4000$, but this is long enough for the first case to show its asymptotic value. The second case continues to fall with increasing k thus implying $\lambda = 0$ (cf. Eq. (14)). As previously discussed, positive λ indicates chaotic motion while $\lambda = 0$ occurs for regular motion.

As an aid in visualizing trajectories in our four-dimensional state space, we employ Poincaré surface of sections. In our case, these are constructed by noting the values of r, ψ, and v whenever the trajectory passes $z = 0$ (or integer multiple of $2L$) with a positive velocity. We then plot ψ versus r (with ψ constrained to be between $-\pi$ and π) and v

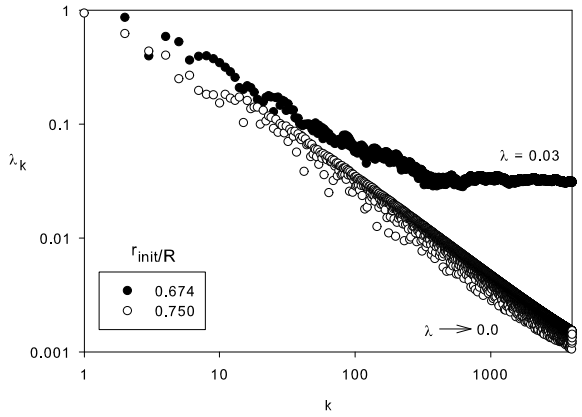

FIGURE 1. Obtaining the Lyapunov exponent for two different initial values of r/R using the method of reference [5].

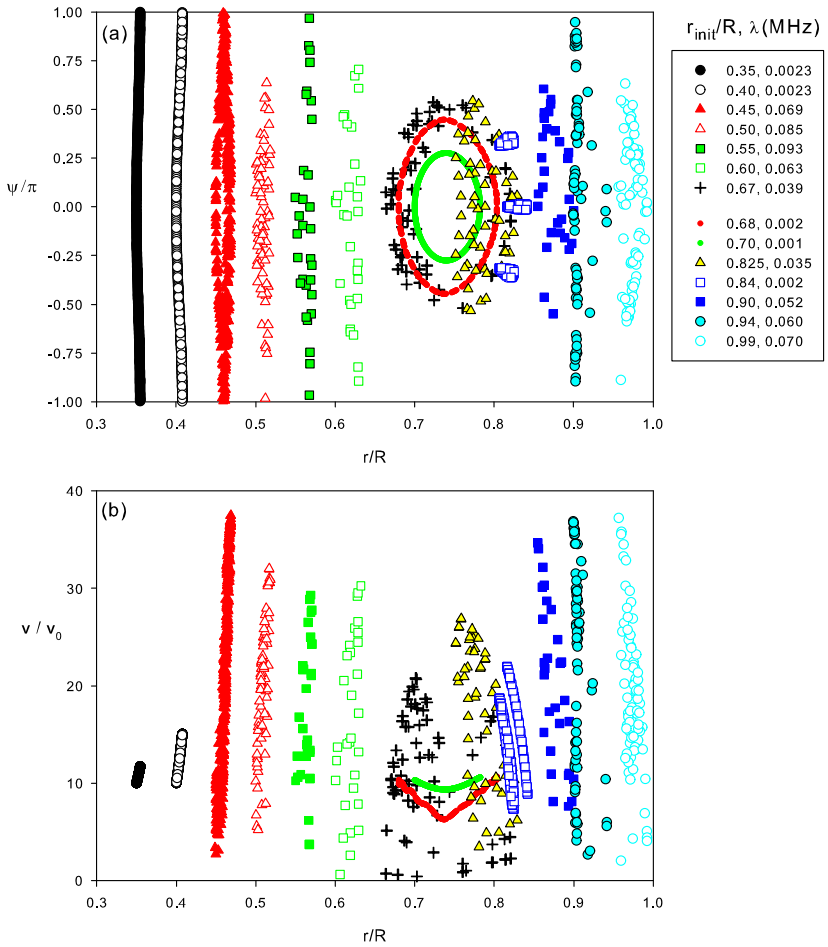

FIGURE 2. (Color online) Poincaré sections taken at the $z = 0$ crossing for fourteen different initial r values through time $t = 6000$. a) Plot of normalized ψ versus r. Legend shows the initial r values and the corresponding Lyapunov exponent λ. b) Plot of normalized v versus r for the same initial r values.

versus r. The resulting plots depend on the selected initial conditions. A representative example is shown in Fig. 2. Initial conditions are $v = 10$, $\psi = 0$, and $z = -0.05$ (as for Fig. 1) and we plot several initial values of r/R on the same graph. The legend gives these initial r/R values and the value of λ_k at the end of the solution. In accord with the behavior seen in Fig. 1, any $\lambda \leq 0.003$ should be considered zero. The code is run to $t = 6000$ to get a reasonable number of points.

A number of interesting features are apparent in both plots. Starting at the smallest initial r values, we see regular motion with little variation in r or v. Then from $r_{init} = 0.45$ to 0.67 the motion is chaotic with larger variations in r and v. Of particular note is the $r/R = 0.67$ case which has large radial excursions. The ellipses in Fig 2a represent the regular motion of particles axially trapped in the asymmetry potential; they are centered on the elliptical fixed point found in the previous section. We have chosen the initial value $r/R = 0.68$ because this gives the largest radial excursion with regular motion. Note that, although the ellipses have large radial excursions, the velocity varies little from the initial value of $v = 10$. At larger r_{init} values, the motions again becomes chaotic with large v variations, with the exception of $r_{init} = 0.84$ with $\lambda \approx 0$ and its symbols clustered in three groups.

Of course, the Poincaré sections shown in Fig. 2 are only a sample since the details depend on the full set of initial conditions and the parameters. More extensive results will be included in a planned longer paper to follow, but some general features can be mentioned here. The parameter ω determines the center of the ellipses in the $\psi - r$ section via the condition $\omega \approx \omega_R(r)$; as ω increases (decreases), the center moves to the left (right). The size of the ellipses is determined by the parameter ϕ_{10} and the location of the center. The chaotic cases occur when the initial v is small (roughly, less than 40), and this appears to be related to the resonance overlap condition for the velocity resonances produced by the counter-propagating helical waves into which the asymmetry can be decomposed[1].

Finally, we note that the chaotic cases shown in Fig. 2 have λ in the range 35-93 kHz which introduces a time scale for collisionless mixing of the orbits that is comparable to other characteristic time scales (azimuthal rotation and axial bounce times). Similar situations have been noted in the astrophysics literature to have significant effects[6, 7]. The effect of chaos on transport in plasmas has been studied for some time[8] but it has not, to our knowledge, been considered in the context of non-neutral plasmas.

Conclusions

We have applied some of the tools of chaos theory to a system of equations describing motion in our cylindrical Malmberg-Penning trap. The problem was re-conceptualized as describing motion on a three-dimensional hypersurface in a four-dimensional space with one constant of the motion. Fixed point analysis reveals elliptical, hyperbolic, and mixed behaviors. We used the technique of Benettin et. al. to calculate Lyapunov exponents which shows that both regular and chaotic motion occur in our system, and this was illustrated with example Poincaré sections.

ACKNOWLEDGMENTS

The author acknowledges the assistance of Kayla Currier and Quinn Taylor and support from Occidental College.

REFERENCES

[1] D. L. Eggleston, Phys. Plasmas **14**, 012302 (2007).
[2] For an example of our experimental work, see D. L. Eggleston and B. Carrillo, Phys. Plasmas **10**, 1308 (2003).
[3] G.L. Baker and J.P. Gollub, *Chaotic Dynamics an Introduction*, (Cambridge, New York, 1990), p. 3.
[4] Michael Tabor, *Chaos and Integrability in Nonlinear Dynamics: An Introduction*, (Wiley, New York, 1989), pp. 20-25.
[5] G. Benettin, L. Galgani, and J-M. Strelcyn, Phys. Rev. A **14**, 2338 (1976); G. Benettin and J-M. Strelcyn, Phys. Rev. A **17**, 773 (1978); Giancarlo Benettin, Luigi Galgani, Antonio Giorgilli, and Jean-Marie Strelcyn, Meccanica, **15**, 9 (1980).
[6] George Contopoulos, *Order and Chaos in Dynamical Astronomy*, (Springer, New York, 2004), pp. 508-13.
[7] D. Pfenniger, Astron. Astrophys., **165**, 74 (1986).
[8] See, for example, G.M. Zaslavsky, Physics Reports **371**, 461 (2002) and references contained therein.